International Journal of Mechanical, Industrial and Aerospace Sciences
ISSN: 2517-9950
Vol:6, No:7, 2012

Stresses Distribution in Spot, Bonded, and Weld-Bonded Joints during the Process of Axial Load

Essam A. Al-Bahkali, Mahir H. Es-saheb, Jonny Herwan

Abstract**—**In this study the elastic-plastic stress distribution in weld-bonded joint, fabricated from austenitic stainless steel (AISI 304) sheet of 1.00 mm thickness and Epoxy adhesive Araldite 2011, subjected to axial loading is investigated. This is needed to improve design procedures and welding codes, and saving efforts in the cumbersome experiments and analysis. Therefore, a complete 3-D finite element modelling and analysis of spot welded, bonded and weld-bonded joints under axial loading conditions is carried out. A comprehensive systematic experimental program is conducted to determine many properties and quantities, of the base metals and the adhesive, needed for FE modelling, such like the elastic – plastic properties, modulus of elasticity, fracture limit, the nugget and heat affected zones (HAZ) properties, etc. Consequently, the finite element models developed, for each case, are used to evaluate stresses distributions across the entire joint, in both the elastic and plastic regions. The stress distribution curves are obtained, particularly in the elastic regions and found to be consistent and in excellent agreement with the published data. Furthermore, the stresses distributions are obtained in the weld-bonded joint and display the best results with almost uniform smooth distribution compared to spot and bonded cases. The stress concentration peaks at the edges of the weld-bonded region, are almost eliminated resulting in achieving the strongest joint of all processes.

Keywords**—**Spot Welded, Weld-Bonded, Load-Displacement curve, Stress distribution

I. Introduction

WELDING is a well-known fabrication process and established manufacturing technique in industry. However, weld-bonding process, which is a combination of the conventional resistance spot welding and adhesive-bonding, is increasingly used in many industries such as automobile, aerospace, home appliances etc. It offers significant improvements in static, dynamic and impact toughness properties of sheet metal joints. Also, it improves the corrosion, noise resistance and stiffness of the joint [1] and can be used for joining dissimilar materials [2], [3]. Therefore, a full understanding of these processes is a must for the joints design and automation of manufacturing, particularly the bond welding process. Also, the modelling and analysis of these processes proves to be of prime importance, though it is complex.

In the last few decades, vast amount of experimental, theoretical and numerical research works is conducted and reported particularly for spot welded and adhesive bonded joints.

Essam A. Al-Bahkali is with the Mechanical Engineering Department, King Saud University, P.O. Box 800, Riyadh 11421, Saudi Arabia (phone: +9661-467-6675; fax: +9661-467-6652; e-mail: ebahkali@ ksu.edu.sa).

Mahir H. Es-saheb is with the Mechanical Engineering Department, King Saud University, P.O. Box 800, Riyadh 11421, Saudi Arabia (phone: +9661-467-6830; fax: +9661-467-6652; e-mail: essaheb@ ksu.edu.sa).

Jonny Herwan is with the Mechanical Engineering Department, King Saud University, P.O. Box 800, Riyadh 11421, Saudi Arabia (e-mail: jherwan@ ksu.edu.sa).

2D and 3D Finite element analyses (FEA) have been widely used in modelling these joining methods [4]-[12]. However, one important aspect, which to date does not receive the needed due attention, is the knowledge of the stresses distributions at all levels of elastic and plastic loadings of these joints particularly the weld-bonded joints. These are required in order to assess the joint performance and application limits. This important issue is not systematically investigated neither reported in literature. Very few scattered works are reported in the elastic region only, for spot welded and bonded joints. Amongst these are the study of the stress distributions of spot welding conducted by Hou et al. [13] and Deng et al. [14] who developed a 3D FE model to study the stress distribution at various ratios of sheet metal thickness and spot weld nugget diameter. Recently, using FE method, load-displacement curve of weld-bonded steel has been plotted by Al-bahkali et. al. [15] and Herwan [16]. Unfortunately, little work is reported in the area of bond welding process. Therefore, to improve design procedures and welding codes, a more systematic investigation covering all stresses distributions, particularly for weld bonding, are essential. Also, achieving representative theoretical models for this process is very important in saving efforts, in the cumbersome experiments and analysis, and has a positive impact on the manufacture and further design of joining. These issues and others are addressed in this investigation. The details of the FEA and experimental procedures and techniques used are given in the next sections.

II. Material and Experimental Techniques

The material of the base metal used in this work is austenitic stainless steel (AISI 304) sheet with 1.00 mm thickness. The mechanical properties of this material are found to be: Modulus of Elasticity 193.7GPA; Yield Stress 277.3MPa and; Ultimate Stress 729.2MPa. These are the average values obtained from the standard tensile tests performed on three standard samples of this material according to ASTM standard E8-81 [17].

The spot welding machine used in this research, for the preparation of spot welded specimen joints, is Meruit Resistance Spot Welding Machine (75kVA). The welding electrodes are water-cooled conical copper alloy electrodes, with contact surface of 4.5mm in diameter. The welding parameters used to fabricate the spot welded joints [1] are: Electrode Pressure 600N; Welding Time 0.2Sec/cycle; Welding Current 6.5kA and; Heat 90 percent.

Epoxy adhesive Araldite 2011 is used for bonding to fabricate both adhesive bonded and weld-bonded lap joint specimens. The mechanical properties of this adhesive as received [18] are: Flexural Modulus 1.904GPa; Flexural Strength 60.4MPa; Poisson Ratio 0.37; Density 1.05g/cm^3

and; Lap Shear Strength 22MPa. The adhesive, used for bonded and weld-bonded joint samples, is prepared by mechanical mixing of resin and hardener in equal amount of volume. Then, the faying surfaces were put in proper position (lap shear joint) after the application of adhesive with uniform thickness layer of 0.1 mm by manual rolling. Finally the joints were cured at 120^0C for 60 minutes to obtain coherent joints.

Again, the weld-bonded specimen joints are prepared, from the polished and cleaned stainless steel sheets, using the same techniques of the adhesive bonded joints followed immediately by resistance spot welding and subsequent curing as stated above. However, the same spot welding parameters are used, except the welding time is increased to become 0.3sec (18 cycles) to overcome the effect of adhesive layer.

In order to obtain the needed elastic-plastic properties required by the FE modeling, microhardness measurements across the joint specimens are made. Vickers micro-hardness measurements of the weld nugget, HAZ, and base metal of spot welded joints is carried out at a load of 100 gram. The measurements started from the center of the nugget moving outwards step by step to the heat affected zone then the base metal, the incremental distance of 0.25 mm is used. But to obtain the plastic properties of each region, spherical indentation (using spherical indenter with 2 mm diameter) is carried out at several loads between 10 to 80kgf. Consequently, the true stress-true strain curves for the materials in these regions are derived using Ahn-Equation [19], given as:

$$\sigma = \left(\frac{1}{\psi}\right) P_m = \left(\frac{1}{\psi}\right)\left(\frac{P}{\pi a_c^2}\right) \quad (1)$$

$$\varepsilon = \left(\frac{\alpha}{\sqrt{1-(a_c/R)^2}}\right)\left(\frac{a_c}{R}\right) \quad (2)$$

Where σ is the true stress, ψ is a plastic constrain factor equal to 3.6 verified by the material tensile test. P is the load, P_m is the mean pressure, a_c is the contact radius between the indenter and the material, ε is the true strain, α is the adjustment constant taken as 0.14, and R is the indenter radius.

The standard shear tensile test of all lap shear joint specimens of the bonded, spot welded, and weld-bonded joints is carried out on an Instron Machine (series 3385H) at 1 mm/min crosshead speed.

Furthermore the ductile fracture limit data are needed to conduct the numerical study of fracture initiation using ABAQUS package. The data are usually expressed in terms of stress triaxialities vs. equivalent strains [20]-[24]. Therefore, to obtain these data, a series of tensile tests (five tests in total) on several notched tensile specimens, and FE-Model of the tensile test of these specimens are conducted. In total, five specimens were prepared and used with notch radii varied between 2 to 5 mm. Then, the equivalent strains are determined from the tensile test data, and the corresponding stress triaxialities are evaluated by the FE model.

III. Finite Element Modeling and Boundary Conditions

A. Geometric Models

A 3D finite element model is developed for each joint type namely: spot welded, bonded, and weld-bonded as well as the base material tensile specimen. Fig. 1 shows the configuration, dimensions, constraints and loading conditions for both bonded and weld-bonded models. The total length of the models used is 175mm and each strip has a thickness of 1.0mm.

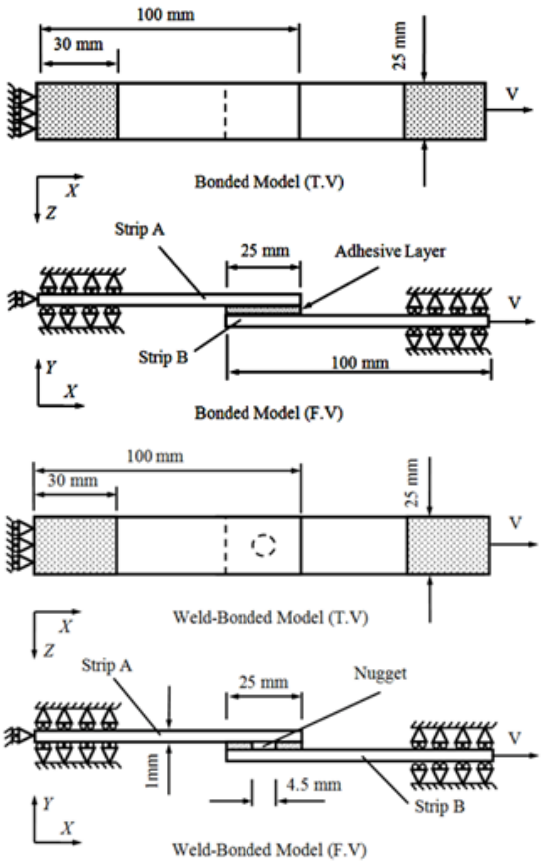

Fig. 1 Finite element models for bonded and weld-bonded joints

B. Analysis Assumptions

The following assumptions were considered: The problem is modelled using three-dimensional FE analysis, and due to symmetry along the center line of the joints, half of the joint is only considered to save computation time. The adhesive layer is assumed to be isotropic. The dimensions of the nugget and HAZ are defined from the micro-hardness measurements. Also, the nugget size is verified from the measurements of the fractured specimen of spot welded joints. The zones are connected with each other by sharing the nodes. The elastic-plastic properties of each zone are introduced based on the material tensile test results for the base metal and the spherical indentation measurements for the nugget and HAZ.

Finally, the adhesive layer is modeled and developed using traction separation mode, since the fracture occurred at the interface between stainless steel and the adhesive layer.

C. Boundary Conditions

The mechanical boundary conditions associated with each finite element model can be summarized as the following:

Symmetric boundary conditions are applied along the x-axis side. As a result of that, two constraints are imposed. The rotation and horizontal displacement at the line of symmetry are zero.

On the left edges at x=0, a clamped boundary conditions are imposed. Thus, the displacements become:

$$u_x = u_y = u_z = 0 \quad (3)$$

Whereas both strips are subject to a fixed y-direction boundary condition at the beginning 30 mm segment of the left base metal strip (x=0 to 30mm) and at the end 30mm segment of right base metal strip (x=145 to 175mm).

$$u_y = 0 \quad (4)$$

The model is subjected to a constant velocity (V=1mm/min.) at the right edges of right base metal strip.

IV. Finite Element Mesh

The finite element computation was carried out using ABAQUS explicit [25]. The finite-element meshes of these models are generated using eight-node-linear brick reduced integration elements (C3D8R) for the stainless steel and three dimensional cohesive elements type COH3D8 for the adhesive layer. The mesh of bonded model is straight forward and simpler because of the absence of spot welding, and it reaches mesh independent solution with a relatively coarse mesh. However, the weld-bonded model needs additional finer mesh on the edges of spot weld and adhesive layer to avoid error analysis. The numbers of elements for the different models that used in the current study, after several refined meshes to insure the conversion of the FE results, are given in Table I.

TABLE I
NUMBER OF ELEMENT USED IN DIFFERENT MODELS

Model	Bonded	Spot Welded	Weld-Bonded
Base Model Strips	744	6972	10202
Adhesive Layer	300	-----	1471
Nugget	-----	690	1035

V. Results

A. Load-Displacement Curves

1. FE and Experimental Results of Spot-Welded Joints

Fig. 2 shows the complete load-displacement curves that were obtained from the FE modeling and corresponding experimental results from the actual spot-welded joint. Thus, the FE and experimental results are in good agreement, except at the plastic region where a maximum acceptable error of 2.6 % was observed.

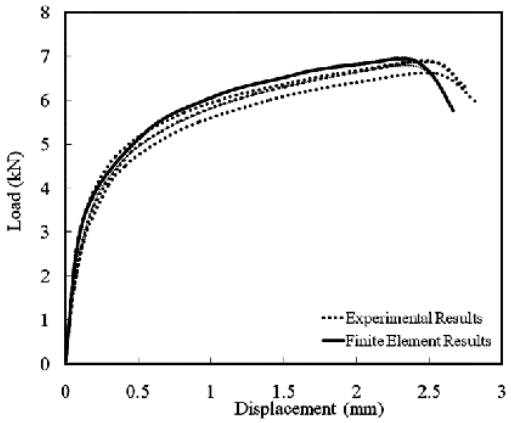

Fig. 2 FE and experimental results of the spot-welded joint

2. FE and Experimental Results of Bonded Joints

The load-displacement curves from the adhesive-bonded joint shear tensile tests are shown in Fig. 3. The experimental and FE results are identical and also show good agreement at the elastic region and fracture initiation (de-lamination) point. The maximum, observed error of 3.82 % at the middle of the plastic region was still reasonable. The mesh refinement was employed to eliminate or reduce these errors but had no effect (already reached mesh independent result). However, the obtained experimental and FE deformation shapes after de-lamination show good agreement.

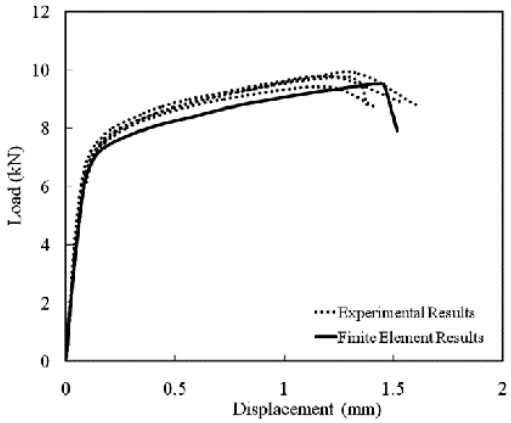

Fig. 3 FE and experimental results of the adhesive welded joint

3. FE and Experimental Results of Weld-Bonded Joints

As stated above, the FE model of the weld-bonded joint was developed by combining the spot-welded and adhesive-bonded joint models. Fig. 4 shows the obtained experimental and FE results. Thus, excellent agreement between the FE results and experimental data at all regions (i.e., elastic, plastic, and fracture initiation point) is attained due to the comprehensive model utilization that was developed from the experimental joint data.

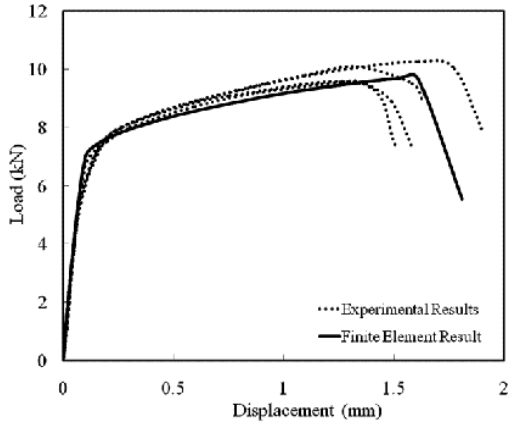

Fig. 4 FE and experimental results of weld-bonded joint

B. Stresses distribution for Spot, Bonded, and Weld-Bonded Joint

The stress distributions were recorded at several load conditions (i.e. elastic, plastic region, and fracture point). These loads are shown in Table II.

TABLE II
LOADS AT WHICH STRESSES ARE RECORDED

Range	Spot Welded	Bonded	Weld-Bonded
Load within elastic limit (N)	280	290	288
	3282	3324	3257
	---	5709	5712
Load within plastic limit (N)	5756	6880	6868
	6882*	9001*	9006*

* Fracture limit load for the model

Fig. 5 shows the normal stress distributions σ_y, the shear stress distribution τ_{xy}, and the Von Mises stress distributions $\sigma_{V.M}$, in a spot welded joint under axial loading at different levels of elastic (two levels of elastic loading) and plastic loads (at the ultimate loading level). The abscissa is in X/L, where X mentioned the position of the stresses from left to right side of the lap joint, and L is the length of lap joint (25mm). Fig. 6 shows the stress distribution in bonded joint under axial loading at different levels of elastic (three loads below elastic limit and two above that limits. Similar arrangement for stress distribution of weld-bonded joints are presented in Fig. 7. Again, in that model, axial loading are at different levels of elastic (three loads below elastic limit and two above it). It is clear from these curves that the stress distribution obtained in the weld-bonded joints, shown in Fig. 7 is more uniform and the edges peak stresses are almost eliminated compared with that obtained in the spot welding and adhesive bonding cases see Figs. 5 and 6.

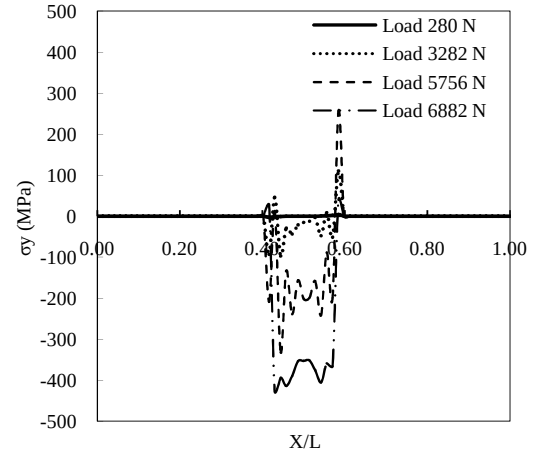

(a) The normal stress distribution (σ_y)

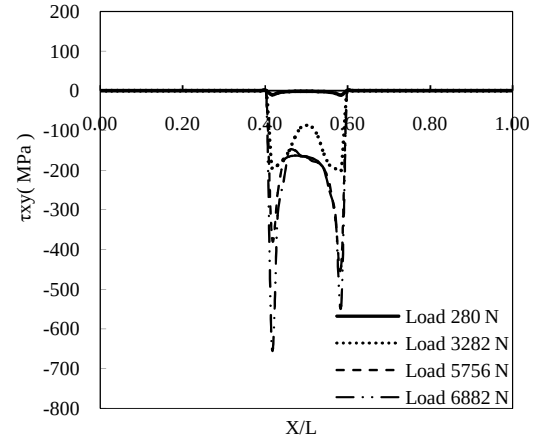

(b) Shear stress distribution (τ_{xy})

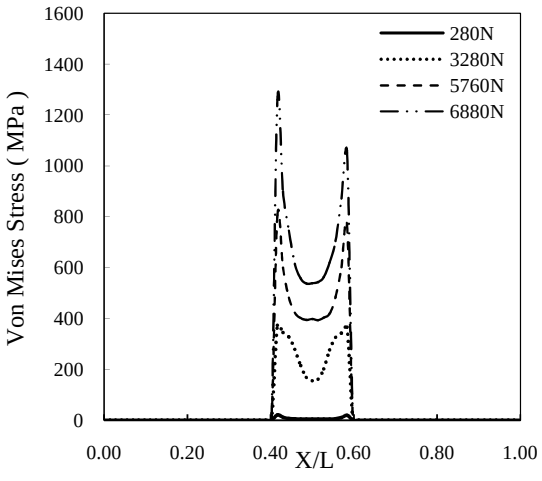

(c) The Von Mises stress distributions ($\sigma_{V.M.}$)

Fig. 5 Elastic-Plastic stresses distribution plots for spot welded joint at the different elastic and plastic loading levels

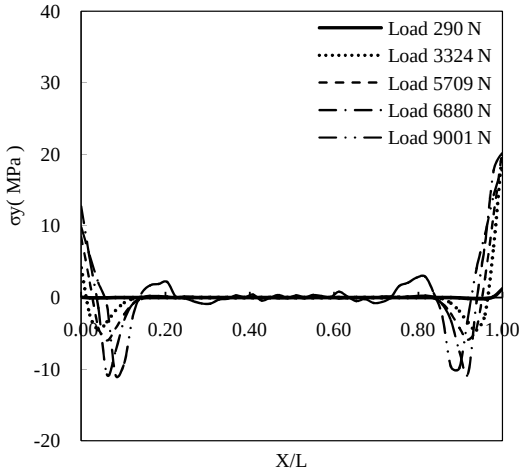

(a) The normal stress distribution (σ_y)

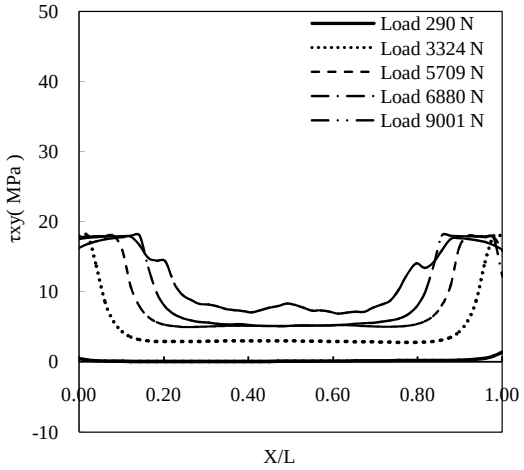

(b) Shear stress distribution (τ_{xy})

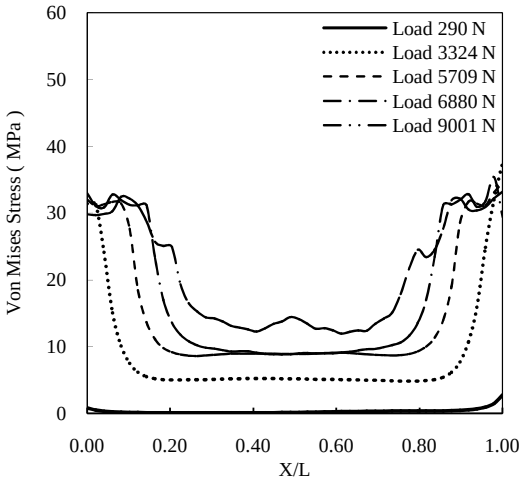

(c) The Von Mises stress distributions ($\sigma_{V.M.}$)

Fig. 6 Elastic-Plastic stresses distribution plots for bonded joint at the different elastic and plastic loading levels

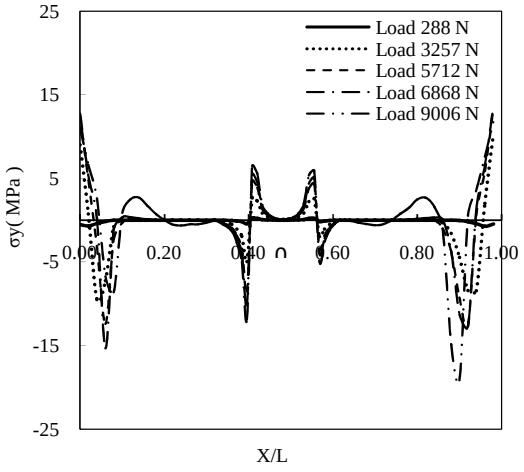

(a) The normal stress distribution (σ_y)

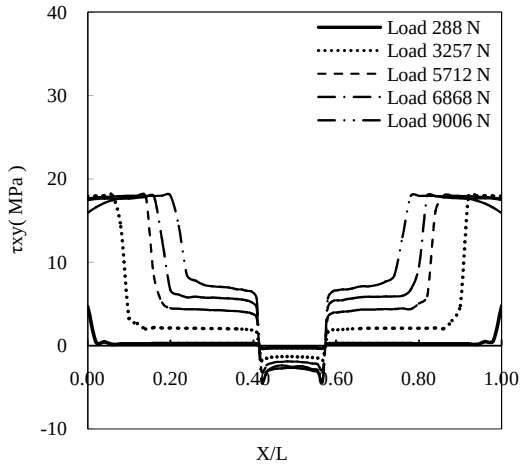

(b) Shear stress distribution (τ_{xy})

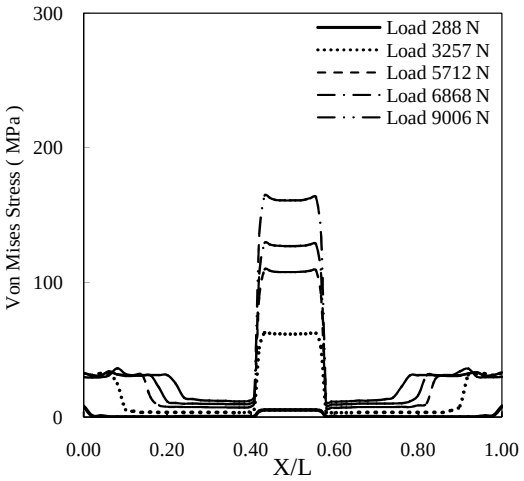

(c) The Von Mises stress distributions ($\sigma_{V.M.}$)

Fig. 7 Elastic-Plastic stresses distribution plots for weld-bonded joint at the different elastic and plastic loading levels

VI. Conclusion

The 3D FE modelling of the three types of spot welded, adhesive bonded and weld bonded are successfully achieved. The load-displacement curves of all three joining types are, also, successfully obtained. In all cases excellent agreement between the results of the FE models and the experimental results is displayed. The deformation modes, fracture initiation point and complete load-displacement curves are obtained.

Using this finite element model, the stress distribution were simulated in term of normal stress, shear stress and Von Mises stress at several point of loads. Through this plotted stress distribution, some phenomena could be explained as follows.

1. The failure of spot welding happened at the interface between weld-nugget and HAZ. This can be explained by Fig. 5, where the Von Mises stress and normal stress in x-direction are very high at these positions.
2. In adhesive bonded joint, the failure (load drop) started whenever the shear stress at the interface between adhesive and base metal reach the maximum value (18 MPa) at 30% area of the lap-joint. This condition happens at the load of about 9kN as shown in Fig. 6. The adhesive joint still can carry the load below this value since the area with maximum shear stress still not reach 30% of the total lap joint area.
3. The effect of adhesive joint in the weld bonded joint is significantly reduced the maximum stress surrounding nugget area as show in Fig. 7. On the other hand the existence of nugget also strengthened the adhesive joint, it can be proved by the increasing the area with maximum shear stress from 30% (in adhesive joint only) to become 40%. Hence, these phenomena can explain the reason why the weld-bonded joint posses the highest strength among the three types of joints.

References

[1] P. K. Ghosh, and Vivek, "Weld-bonding of stainless steel", *ISIJ International*, Vol. 43, pp. 85-94, 2003.
[2] Q. D. Yang, M. D. Thouless, and S. M. Ward, "Elastic-plastic mode-II fracture of adhesive joints", *International Journal of Solids and Structures*, Vol. 38, pp. 3251-3262, 2001.
[3] A. Hasanbasoglu, and R. Kacar, "Resistance spot welding of dissimilar materials (AISI 316L-DIN EN 10130-99)", *Journal of Materials and Design*, Vol. 28, pp. 1794-1800, 2007
[4] I. R. Nodeh, S. Serajzadeh, and A. H. Kokabi, "Simulation of welding residual stresses in resistance spot welding, FE Modeling and X-ray verification", *Journal of Materials Processing Technology*, Vol. 205, pp. 60-69, 2008
[5] A. De, M. P. Thaddeus, and L. Lorn, "Numerical modeling of resistance spot welding of aluminum alloy", *ISIJ International*, Vol. 43, No. 2, pp. 238-244, 2003.
[6] J. Z. Chen, and D. F. Farson, "Analytical modeling of heat conduction for small scale resistance spot welding process", *Journal of Materials Processing Technology*, Vol. 178, pp. 251-258, 2006.
[7] X. Kong, Q. Yang, B. Li, G. Rothwell, R. English, and H. J. Ren, "Numerical Study of spot-welded joints of steel", *Journal of Materials and Design*, Vol. 29, pp. 1554-1561, 2008.
[8] S. L, M. D. Thouless, A. M. Waas, J. A. Schroeder, and P. D. Zavattieri, "Use of mode I cohesive zone models to describe the fracture of an adhesively-bonded polymer-matrix composite", *Journal of Composite Science and Technology*, Vol. 65, pp. 281-293, 2005.
[9] S. Li, M. D. Thouless, A. M. Waas, J. A. Schroeder, and P. D. Zavattieri, "Mixed-mode cohesive-zone models for fracture of an adhesively bonded polymer-matrix composite", *Journal of Engineering Fracture Mechanics*, Vol. 73, pp. 64-78, 2006.
[10] M. You, Z. Li, X. Zheng, S. Yu, G. Li, and D. Sun, "A numerical and experimental study of performed angle in the lap zone on adhesively bonded steel single lap joint", *International Journal of Adhesion and Adhesives*, Vol. 29, pp. 280-285, 2009.
[11] M. N. Cavalli, M. D. Thouless, and Q. D. Yang, "Cohesive-zone modeling of the deformation and fracture of weld-bonded joints", *Welding Journal*, Vol. 83, p. 133S-139S, 2004.
[12] Y. Xia, Q. Zhou, P. C. Wang, N. L. Johnson, X. Q. Gayden, and J. D. Fickers, "Development of high-efficiency modeling technique for weld-bonded steel joints in vehicle structures-part I: static experiments and simulations", *International Journal of Adhesion and Adhesives*, Vol. 29, pp. 414-426, 2009.
[13] Z. Hou, I. S. Kim, Y. Wang, C. Li, and C. Chen, "Finite element analysis for the mechanical features of resistance spot welding process", *Journal of Materials Processing Technology*, Vol. 185, pp. 160-165, 2007.
[14] X. Deng, W. Chen, and G. Shi, "Three-dimensional finite element analysis of mechanical behavior of spot welds", *Journal of Finite Element Analysis and Design*, Vol. 35, pp. 17-39, 2000.
[15] E. Al-bahkali , M. Es-saheb, and J. Herwan, "Finite Element Modeling of Weld-Bonded Joint", *4th International Conference on Advanced Computational Engineering and Experimenting*, Paris, 2010.
[16] J. Herwan, "Load-Displacement Curve Prediction of Weld-Bonded Stainless Steel Using Finite Element Method", MSc thesis, King Saud University, KSA, 2010.
[17] ASTM, "Standard method of tension testing of metallic materials", Annual Book of standard, ASTM-E8-81, 1981.
[18] Huntsman Corp, "Technical data sheet of structural adhesives araldite-201", Huntsman Advanced Materials, 2007.
[19] E. Jeon, J. Y. Kim, M. K. Baik, S. H. Kim, J. S. Park, and D. Kwon, "Optimum definition of true strain beneath a spherical indenter for deriving indentation flow curves", *Journal of Materials Science and Engineering*, Vol. A419, pp. 196-201, 2006.
[20] Y. Bao," Dependence of ductile crack formation in tensile tests on stress triaxiality stress and strain ratios", *Journal of Engineering Fracture Mechanics*, Vol. 72, pp. 502-522, 2005.
[21] M. Alves, and N. Jones, "Influence of hydrostatics stress on failure of axi-symmetric notched specimens", *Journal of the Mechanics and Physics of Solids*, Vol. 47, pp. 643-667, 1999.
[22] A. C. Mackenzie, J. W. Hancock, and D. K. Brown, "On the influence of state of stress on ductile failure initiation in high strength steels", *Journal of Engineering Fracture Mechanics*, Vol. 9, pp. 167-188, 1977.
[23] C. Sun, M. D. Thouless, A. M. Waas, J. A. Schroeder, and P. D. Zavattieri, "Rate effects for mixed-mode fracture of plastically-deforming adhesively-bonded structures", International Journal of Adhesion and Adhesives, Vol. 29, pp. 434-443, 2009.
[24] M. Arai, Y. Noro, K. Sugimoto, and M. Endo, "Mode I and mode II interlaminar fracture toughness of CFRP laminates toughened by carbon nanofiber interlayer", *Journal of Composite Science and Technology*, Vol. 68, pp. 516-525, 2008.
[25] ABAQUS, User's Manual, Version 6.9, 2010.